J Mater Sci: Mater Med (2010) 21:2501–2509
DOI 10.1007/s10856-010-4103-8

Biomimetic transformations of amorphous calcium phosphate: kinetic and thermodynamic studies

D. Rabadjieva · R. Gergulova · R. Titorenkova · S. Tepavitcharova · E. Dyulgerova · Chr. Balarew · O. Petrov

Received: 26 November 2009 / Accepted: 20 May 2010 / Published online: 9 June 2010

Abstract The biomimetic synthesis and phase transformation of XRD amorphous calcium phosphate were studied by application of kinetic, chemical and spectral (XRD and IR) methods and thermodynamic simulations. Two SBFs (SBFc and SBFr), differing in their HCO_3^- and Cl^- ion contents, were used in the maturation studies. It has been proven that the biomimetic maturation accelerated the phase transformation of less thermodynamically stable amorphous calcium phosphate to poorly crystalline hydroxyapatite. Several regularities have been found: (i) kinetic reasons determined the biomimetic precipitation of XRD-amorphous calcium deficient phosphate (ACP); (ii) the precipitated ACP always contained impurities due to co-precipitation, ion substitution and incorporation phenomena; (iii) the increased content of HCO_3^- ions in the surrounding microenvironments increased the rate of phase transformation and the concentration of $MeHCO_3^+$ (Me = Ca, Mg) species in the solution, but the solubility of $CaCO_3$ has only been decreased and its precipitation accelerated, thus playing a crucial role in the process under study.

D. Rabadjieva (✉) · R. Gergulova · S. Tepavitcharova · Chr. Balarew
Institute of General and Inorganic Chemistry, Bulgarian Academy of Sciences, Acad. G. Bontchev Str., Bl.11, Sofia, Bulgaria
e-mail: didiarab@svr.igic.bas.bg

R. Titorenkova · O. Petrov
Central Laboratory of Mineralogy and Crystallography, Bulgarian Academy of Sciences, Acad. G. Bontchev Str., Bl.107, 1113 Sofia, Bulgaria

E. Dyulgerova
Dental Medicine Faculty, University of Medicine, 1 G. Sofiiski Str, 1431 Sofia, Bulgaria

1 Introduction

The biomimetic approach has become a modern way to the elucidation of some of the elementary processes of hard tissue mineralization and for testing bone-bonding properties of bioactive materials. Poorly crystalline apatites are involved in many biological systems, in processes of mineralization [1], calcium phosphate coating layers on bone implants [2–7], etc. Although they play a key role in the bioactivity of the bone-bonding processes, their physical–chemical properties are not well known because of their reactive instability and difficulties in characterization of nanosized crystals.

Electrolyte solutions with different compositions, referred to as "simulated body fluids" (SBFs), which claim to mimic the cellular human body plasma, have been proposed and used for in vitro studies. Kokubo [8] has popularized SBF, called conventional (SBFc), containing definite amounts of Na^+, K^+, Mg^{2+}, Ca^{2+}, Cl^-, HCO_3^{2-}, HPO_4^{2-} and SO_4^{2-} ions, and having a Ca/P ratio of 2.5 (equal to that in blood plasma), a HCO_3^- concentration of 4.2 mmol dm^{-3} and physiological pH (7.3–7.4). To better mimic the blood plasma, Bayraktar and Tas [9] have revised Kokubo's SBFc by increasing the concentration of HCO_3^- ions up to 27 mmol dm^{-3} at the expense of Cl^- ions (referred to as SBFr). Marques et al. [10] have also reported a physiological carbonate–hydrogen carbonate buffered Carbonated Simulated Inorganic Plasma (CSPI) with a HCO_3^- concentration in the range of 24–27 mmol dm^{-3}. In contrast to SBFs, the blood plasma contains a mixture of buffer systems such as HCO_3^-/CO_2, $HPO_4^{2-}/H_2PO_4^-$ and protein/Hprotein, the HCO_3^-/CO_2 equilibrium being of major importance for its buffer capacity [11]. Despite these differences, the precipitation processes of bioactive calcium phosphate in simulated

body fluids and the influence of the medium composition on its formation and phase transformation have attracted extensive research interest [3, 4, 7, 12–15], because of their analogy to the biological mineralization process.

The purpose of this work is to study the biomimetic synthesis and phase transformation of amorphous calcium phosphate by kinetic, spectral and thermodynamic research and to explain the role of HCO_3^- ions in these processes.

2 Materials and methods

2.1 Solutions

2.1.1 Simulated body fluids (SBFs)

All the SBFs used in this study (Table 1) were prepared by successive mixing of preliminary prepared solutions of KCl, NaCl, $MgCl_2 \cdot 6H_2O$, $CaCl_2 \cdot 2H_2O$, $NaHCO_3$, Na_2SO_4, and K_2HPO_4 or Na_2HPO_4 salts in deionised water. The pH of the mixed solutions was adjusted to 7.2–7.4 using 0.1 M HCl or 0.05 M Tris (hydroxymethyl) aminomethane.

(i) SBFs used in the precipitation processes
To avoid preliminary precipitation, modified calcium-free (SBFc-*Cam*) as well as phosphorous-free (SBFc-*Pm*)) conventional simulated body fluids (SBFc) were used as solvents for K_2HPO_4 and for $CaCl_2$, respectively.

(ii) SBFs used in the maturation processes
A conventional simulated body fluid (SBFc) was prepared according to Kokubo [8].
A revised simulated body fluid (SBFr) was prepared according to Bayraktar and Tas [9].

Table 1 Inorganic composition of human plasma and simulated body fluids (SBF) (mmol dm^{-1})

Composition	Human plasma [8]	SBFc [8]	SBFr [9]	SBFc-*Pm* ($CaCl_2$ solution)	SBFc-*Cam* (K_2HPO_4 solution)
Na^+	142.0	142.0	142.0	141.9	141.9
K^+	5.0	5.0	5.0	5.0	383.5
Mg^{2+}	1.5	1.5	1.5	1.5	1.5
Ca^{2+}	2.5	2.5	2.5	567.0	0.00
Cl^-	103.0	147.8	125.0	1271.9	142.8
SO_4^{2-}	0.5	0.5	0.5	0.5	0.5
HCO_3^-	27.0	4.2	27.0	4.2	4.2
HPO_4^{2-}	1.0	1.0	1.0	0.00	190.2

2.2 Synthesis and phase transformations

2.2.1 ACP biomimetic precipitation

The samples of amorphous calcium phosphate were precipitated by quick mixing of solutions of $CaCl_2$ and K_2HPO_4, where the Ca/P ratio was 1.67. Both salts were initially dissolved in appropriately modified conventional simulated body fluids (SBFc-*Pm* and SBFc-*Cam*). The precipitation was conducted in a medium with pH 11.5 (controlled by 1 M KOH), at room temperature and under intense stirring. The precipitate was filtered and immediately washed with water and with acetone (solid-to-liquid ratio of 1:1) and then freeze-dried (-18 ± 1°C, under silica gel) for a week.

2.2.2 ACP biomimetic maturation

Two series of experiments were done: with SBFc and with SBFr. The freeze-dried precipitates were matured in SBFs with a solid-to-liquid ratio of 1:250 in closed plastic vessels. The solid samples were kept in the solutions for 0.3, 1, 2, 4, 6 and 72 h, respectively at a temperature of 37 ± 0.5°C under static conditions. There were also samples kept in the solution for 720 h (30 days), the matured SBFs having been replaced regularly twice a week starting from the 3rd day (72nd hour).

2.3 Characterization

2.3.1 Chemical analysis

Following the kinetics of maturation, the solids and their liquid phases were regularly analyzed. The sum of Ca^{2+} and Mg^{2+} ions was determined complexometrically by EDTA at pH 10. The concentrations of Mg^{2+}, K^+ and Na^+ ions were measured by a TERMO M5 atomic absorption spectrometer, and those of P–PO_4^{3-} and Cl^- ions, by a NOVA 60 spectrophotometer using Merck and Spectroquant® test kits.

2.3.2 X-ray diffraction

The polymorphous phase transformations and the crystallinity of calcium phosphates were determined by a Bruker D8 advance XRD, operating at 40 kV and 40 mA with Cu K_α radiation and a SolX detector within the 2θ range of 10–90° 2θ, step 0.04° 2θ and counting time 1 s/step. A WinFit computer program [16] was used to evaluate the crystal size as a function of the maturation process duration.

2.3.3 IR spectroscopy

The spectra of solid samples were collected by a Tensor 37 FTIR spectrometer in the 400–4,000 cm^{-1} spectral range

with a 4 cm^{-1} spectral resolution after averaging 72 scans on standard KBr pallets. Absorption spectra were baseline corrected via rubber band correction, min–max normalized and smoothed at 9 points. For a more precise study of the amorphous calcium phosphate transformations during the first 3 h of maturation, IR spectra were registered periodically every 20 min. OPUS 5.5 was used for spectra evaluation.

2.3.4 Thermodynamic simulations

A computer program PHREEQCI v.2.14.3 [17], based on an ion-association model was used to simulate both the precipitation and maturation processes. All possible association/dissociation and dissolution/crystallization processes in SBFs were taken into account. The formation of complexes and the salt precipitation were defined via a mass-action expression with appropriate formation constants or solubility products. The activity coefficients of all possible simple and complex species were calculated using the extended Debye–Huckel theory. An updated database [18] was used.

The saturation indices (SI) (Eq. 1), calculated under the experimental conditions were used as indicators for possible salts crystallization,

$$SI = \lg(IAP/K) \quad (1)$$

Here, IAP is an ion activity product and K is a solubility product.

In the calculation, we used data by Fernández [19] and Dorozhkin [1] for the solubility products of calcium phosphates.

The species distribution was calculated using the ratio $[MX_i]/[M_{tot}]$ with $[MX_i]$ and $[M_{tot}]$ being the concentration of the species and the total metal concentration, respectively.

3 Results and discussion

Chemical syntheses and analyses, kinetic and spectral (powder XRD and IR) studies, and thermodynamic modeling were applied to follow the processes of biomimetic synthesis of amorphous calcium phosphate and its phase transformations. Two SBFs (SBFc and SBFr), differing only in the content of HCO_3^- and Cl^- were used to explain the role of HCO_3^- ions in the maturation process.

3.1 ACP biomimetic synthesis

Various crystal chemical and kinetic factors determine the crystallization process. It starts when some of the complexes existing in the solution possess a sufficiently high activity to reach and surpass the solubility product of the crystallizing salt. This means that important for the crystallization process is the activity of definite entities in the solution (complexes, molecules, or simple ions) that are able to be incorporated in the crystal directly or with minor changes. The crystallization of calcium hydroxyapatite, $Ca_{10}(PO_4)_6(OH)_2$, could occur in two stages: precipitation of a metastable amorphous product and its re-crystallization to calcium hydroxyapatite. The fast mixing, high supersaturation and the presence of Mg^{2+} and CO_3^{2-} ions provoke precipitation of an amorphous calcium deficient product [20–22]. The applied approach of biomimetic precipitation ensures these conditions and allow obtaining XRD-amorphous (Fig. 1) calcium deficient phosphate (ACP) with a Ca/P ratio of 1.51 (Table 2), although the medium pH (11.5) and the Ca/P ratio (1.67) were chosen so as to favor the formation of a hydroxyapatite.

The SBF, as an electrolyte medium, plays a crucial role in the precipitation processes and influences the composition of the precipitated product. Precipitation, co-precipitation, ion substitution and ion incorporation reactions take place simultaneously. The cationic and anionic substitutions are mainly responsible for the calcium deficiency of the precipitated ACP. Posner et al. [23, 24] have explained the calcium deficiency assuming the formation of $Ca_9(PO_4)_6$ clusters as a first step in the mechanism of ACP formation. The CO_3^{2-} ions from the solution compete with and partially replace the PO_4^{3-} ions in the structure following, however, the rule for electrostability that results in a structure with Ca vacancies. Part of these calcium vacancies could be occupied by free Na^+, K^+ and Mg^{2+} ions from the solution, thus forming Posner's clusters with the common formula $Ca_wMg_xNa_yK_z(PO_4)_v(CO_3)_{6-v}$ $(w + x + y + z < 9)$.

In SBF, different calcium, magnesium, sodium and potassium salts could co-precipitate along with ACP. Our thermodynamic calculations of the Saturated Indices (SI) of all the solid phases which may exist in the medium showed co-precipitation of only 9 salts with positive SI, namely $Mg(OH)_2$, $CaHPO_4$, $Mg_3(PO_4)_2{\cdot}8H_2O$, $MgCO_3{\cdot}Mg(OH)_2{\cdot}3H_2O$, $CaCO_3$, $Ca_3(PO_4)_2$(am), $Ca_8H_2(PO_4)_6{\cdot}5H_2O$, $Ca_9Mg(HPO_4)(PO_4)_6$ and $Ca_{10}(PO_4)_6(OH)_2$ (Table 3). The highest SI and thermodynamic stability are displayed by hydroxyapatite ($Ca_{10}(PO_4)_6(OH)_2$) followed by whitlockite ($Ca_9Mg(HPO_4)(PO_4)_6$), but the quick kinetic favors the formation of amorphous phases. This result is in compliance with Ostwald's step rule, according to which the crystal phase that nucleates, is not the phase that is most thermodynamically stable under these conditions, but rather is a metastable phase closest in free energy to the parent phase [25]. The highest crystallization rate and the lowest supersaturation, necessary for nucleation, should be exhibited by the salts for which, in the saturated solution, there is a sufficient concentration of structural entities able to be incorporated unchanged or with small changes into the crystal structure.

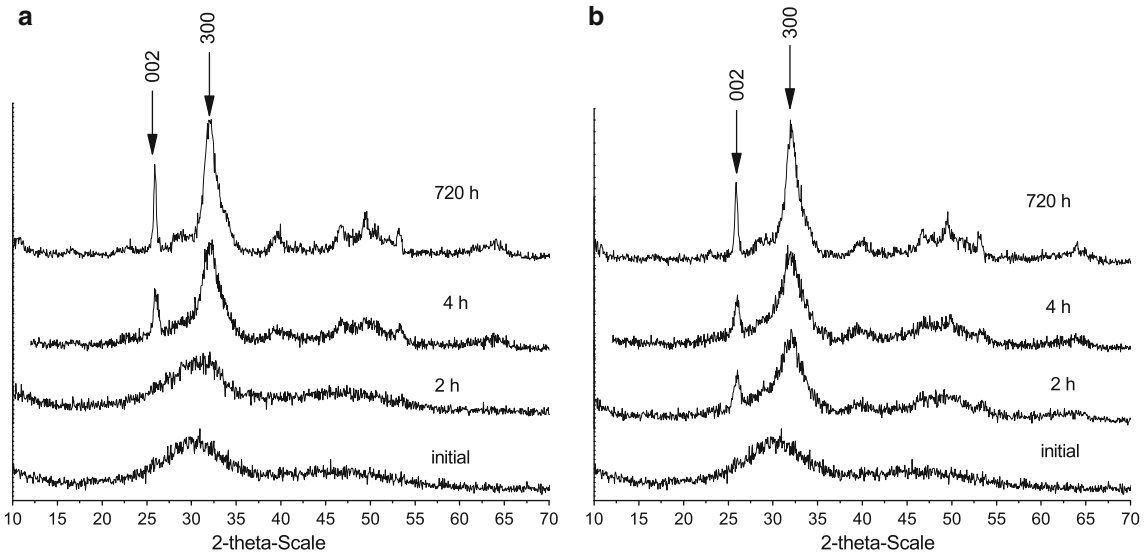

Fig. 1 XRD powder data of solid phases after different maturation times: **a** SBFc; **b** SBFr

Table 2 Compositions of the initial precipitated ACP and natural enamel, dentin, cementum and bone

Mg (mmol/g)	Na (mmol/g)	K (mmol/g)	Cl (mmol/g)	Mg/Ca	Ca/P	(Ca + Mg + Na + K)/P
Biomimetic precipitated ACP						
0.13	0.20	0.45	0.03	0.03	1.51	1.79
Enamel, dentin, cementum, bone [1]						
0.02–0.29	0.22–0.39	2×10^{-4}–0.02	0.03–0.1	0.03–0.06	1.61–1.77	

Thus, the ionic substitution, co-precipitation as well as the additional easy incorporation of maternal solution in the aggregates lead to precipitation of calcium deficient phosphate with a (Ca + Mg + Na + K)/P ratio of 1.79 that is higher than those of calcium *ortho*-phosphates (maximum Ca/P ratio of 1.67 for hydroxyapatite). Its mineral composition was found to be similar (with the exception of the Ca/P ratio and the K content) to those in the hard tissues enamel, dentin, and bone mineral [1] (Table 2).

IR spectra of the initially precipitated ACP exhibit an intense peak at 1,050 cm^{-1}, which is due to antisymmetric P–O stretching (v_3) and another at 570 cm^{-1} due to O–P–O bending vibrations (v_4) (Fig. 2). The peaks in the spectral range 1,420–1,490 cm^{-1} are characteristic of C–O antisymmetric stretching vibrations (v_3) of B type carbonate group, whereas the peak at about 870 cm^{-1} is generated by v_2 of the carbonate group [26].

3.2 ACP biomimetic maturation

3.2.1 Kinetic studies

The kinetic studies of freeze-dried ACP maturation in SBFc as well as in SBFr (with a 6.5 times higher content of HCO_3^-) show changes in the composition of both solid and liquid phases during the first 1.5–2 h of maturation (Fig. 3). The changes in the content of Ca^{2+} and PO_4^{3-} in the solid phases are analogous during all the maturation processes (Fig. 3a), whereas in the liquid phases they are analogous in character but opposite in values for both SBFs. In the solid phases, the contents of Ca^{2+} and PO_4^{3-} ions increase and then remain approximately constant, whereas that of Mg^{2+} first slowly decreases, then quickly increases twice for about 5 h and finally slowly increases about three times. Only small differences are observed between the solid samples matured in both SBFs. During the first 1.5–2 h, the liquid phases are slightly enriched in Ca^{2+} and Mg^{2+}, and significantly in PO_4^{3-} ions (Fig. 3b), after which their contents gradually reduce. The decrease in content of the Ca^{2+} and PO_4^{3-} ions for SBFc is practically equal (50–60%), whereas for SBFr it is about 90% for Ca^{2+} and about 20% for PO_4^{3-} ions. These results reveal that the dissolution/crystallization processes of calcium are strongly influenced by the content of HCO_3^- ions. In SBFr richer in HCO_3^-, crystallization of $CaCO_3$ occurs, confirmed also by the increased Ca/P ratios (Fig. 4), whereas in SBFc the formation of calcium phosphate dominates. For both SBFs, the contents of Mg^{2+} in solid

Table 3 Possible salts in the biomimetic systems and their thermodynamic calculated saturated indices (SI). Case studies of ACP precipitation and ACP maturation

Phase	Co-precipitation	Maturation of *ACP		Maturation of **ACP	
		SBFc	SBFr	SBFc	SBFr
$NaHCO_3{\cdot}Na_2CO_3{\cdot}2H_2O$	−11.65	−9.76	−8.69	−12.95	−9.05
Na_2SO_4	−6.81	−6.15	−6.14	−6.14	−6.13
$Na_2CO_3{\cdot}H_2O$	−6.78	−7.66	−6.94	−10.56	−8.08
$MgSO_4{\cdot}7H_2O$	−6.47	−5.26	−5.84	−5.25	−5.25
$NaHCO_3$	−5.75	−3.53	−3.17	−3.81	−2.4
$Na_2SO_4{\cdot}10H_2O$	−5.45	−5.34	−5.32	−5.33	−5.31
$Mg_5(CO_3)_4(OH)_2{\cdot}4H_2O$	−5.12	−10.95	−10.33	−27.75	−15.76
$Na_2CO_3{\cdot}10H_2O$	−4.9	−6.25	−5.53	−9.15	−6.67
$MgCO_3{\cdot}3H_2O$	−3.54	−3.67	−3.55	−6.56	−4.1
$MgHPO_4{\cdot}3H_2O$	−3.49	−1.01	−0.89	−1.91	−1.21
NaCl	−3.13	−3.59	−3.66	−3.59	−3.65
$CaSO_4$	−1.67	−2.77	−3.48	−2.86	−4.13
$CaSO_4{\cdot}2H_2O$	−1.44	−2.58	−3.28	−2.67	−3.94
$Ca(OH)_2$	−1.39	−9.01	−9.01	−14.34	−13.49
$Mg_3(PO_4)_2{\cdot}22H_2O$	−1.23	−2.3	−1.93	−9.32	−5.8
$Mg_3(PO_4)_2$	−1.08	−2.27	−1.9	−9.29	−5.77
$MgCO_3$	−0.73	−1.17	−1.05	−4.07	−1.6
$KMgPO_4{\cdot}6H_2O$	−0.32	−2.92	−2.43	−6.43	−4.66
$CaMg_3(CO_3)_4$	−0.29	−3.18	−2.81	−14.86	−6.25
$CaHPO_4{\cdot}2H_2O$	−0.15	−0.23	−0.23	−1.23	−1.8
$Mg(OH)_2$	0.11	−5.95	−5.93	−11.05	−9.0
$CaHPO_4$	0.14	0	0	−1.05	−1.61
$Mg_3(PO_4)_2{\cdot}8H_2O$	0.78	−0.37	0	−7.14	−3.77
$MgCO_3{\cdot}Mg(OH)_2{\cdot}3H_2O$	1.09	−4.41	−4.27	−12.29	−7.75
$CaCO_3$	2.62	0	0	−2.94	−1.77
$Ca_3(PO_4)_2$(am)	8.37	0	−0.10	−6.76	−7.64
$Ca_8H_2(PO_4)_6{\cdot}5H_2O$	26.63			−6.62	−8.43
$Ca_9Mg(HPO_4)(PO_4)_6$	34.19			−11.37	−11.55
$Ca_{10}(PO_4)_6(OH)_2$	60.18			0	0

Note: Possible content of the initial precipitated product—ACP with up to 1–3% impurities

* ACP gives the metastable precipitation ($8.37 > SI > 0$)

** ACP gives the equilibrium system($SI > 0$)

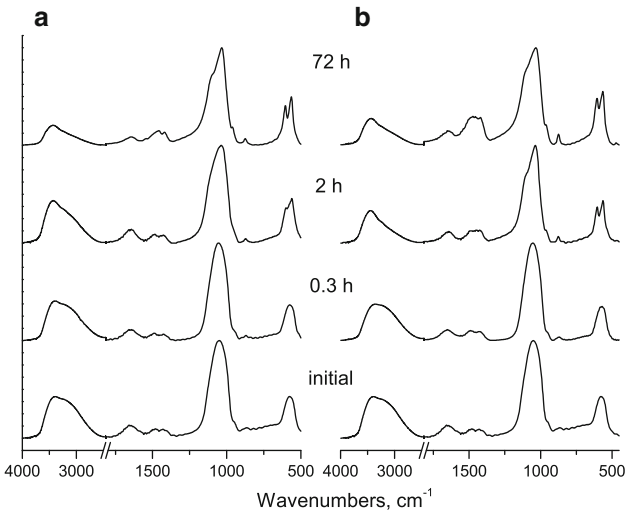

Fig. 2 FTIR spectra of solid phases after different maturation times: **a** SBFc; **b** SBFr

and liquid phases change in a similar way. The higher content of HCO_3^- in SBFr is only responsible for the solution phenomena of co-precipitated magnesium hydroxide and carbonate and for the increasing $MgHCO_3^+$ concentration in the solution. The further incorporation of Mg^{2+} in the amorphous phase and its respective decrease in the liquid phase by about 80% does not depend on the concentration of HCO_3^- ions.

3.2.2 XRD studies

The powder XRD data confirm the initial precipitation of amorphous calcium phosphate and its further biomimetic conversion into more stable poorly crystalline apatite (Fig. 1). The SBF carbonate content was confirmed to increase the rate of phase transformation. Thus, a crystal phase was detected after the 2nd hour of maturation in

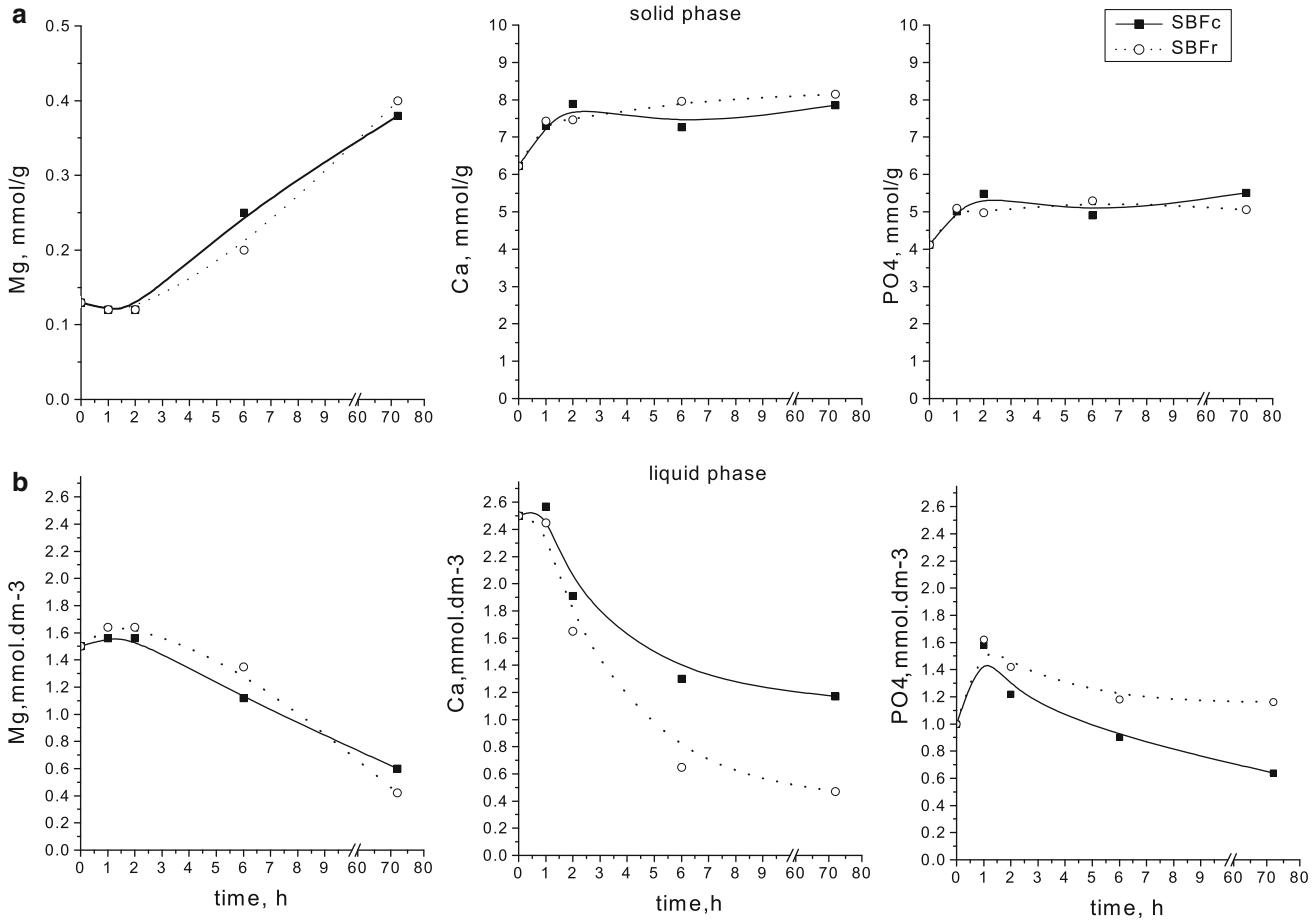

Fig. 3 Kinetics profile of Mg^{2+}, Ca^{2+} and PO_4^{3-} contents in solid (**a**) and liquid (**b**) phases after different maturation times

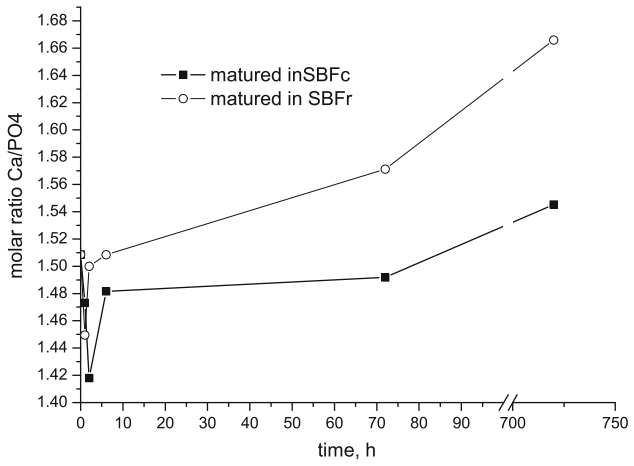

Fig. 4 Ca/P molar ratio in solid phases after different maturation times

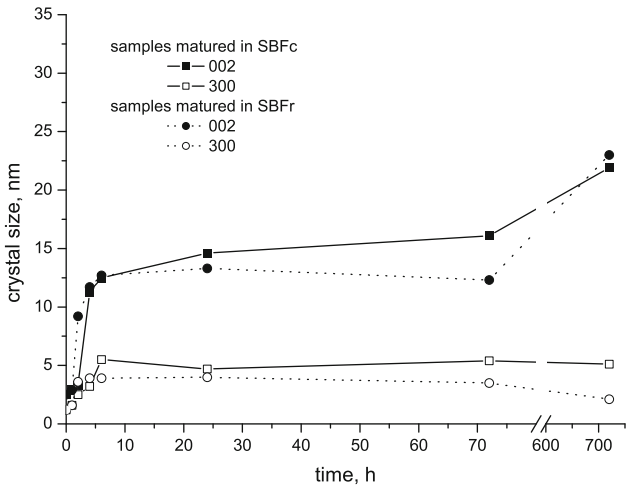

Fig. 5 Calculated crystal size of solid phases after different maturation times

SBFr richer in HCO_3^- ions, while in SBFc this happened 2 h later. The calculated crystal size (in 002 and 300 crystallographic planes) of the matured solid phases (Fig. 5) indicates a small difference between the two SBFs and a slight crystal growth after 72 h of maturation. The crystal size in the plane 002 is 3 times greater than that in the plane 300. The leap after that is due to crystal growth from fresh portions of SBFs.

3.2.3 IR spectroscopy studies

The increase in crystallinity with the duration of maturation is confirmed by the appearance of the splitting of phosphate bands at 960, 1,100, 562, and 603 cm^{-1} which are characteristic for IR spectra of crystalline calcium phosphate (Fig. 2). IR data also revealed a change in the carbonate content of the samples treated in both SBFs (Fig. 6). As a measure of the carbonate content we used the ratio between the areas bellow the peaks corresponding to CO_3^{2-} (1,549–1,336 cm^{-1}) and PO_4^{3-} (1,280–914 cm^{-1}) stretching bands. As seen, the amount of carbonate ions increases faster in samples matured in SBFr than in such matured in SBFc.

3.2.4 Thermodynamic modeling

Thermodynamic simulations of the maturation process of two different solid calcium phosphate products, a metastable amorphous product (*ACP), and a stable equilibrium product (**ACP) were performed in two solutions (SBFc and SBFr) differing in the content of HCO_3^- ions. The metastable amorphous product (*ACP) simulated the system behavior during the first 1–2 h of maturation, when the apatite phase was still not formed, whereas the stable product (**ACP) simulated the equilibrium system. The co-precipitated salts with saturated indices (SI) in the range $8.37 > SI > 0$ are considered as metastable amorphous products (*ACP), while all nine salts with $SI > 0$ are considered as stable equilibrium product (**ACP) (Table 3). The impurities in the washed initial products were taken in the range 1–3% based on the measured Mg/Ca ratio (3 mol%) (Table 2).

The maturation of metastable amorphous product shows a phase transformation that depends on the content of HCO_3^- ions in SBF at the beginning of the process. In a solution with a low HCO_3^- content (SBFc), solubility phenomena of all magnesium salts occur ($SI < 0$) during maturation and the system will be in equilibrium with the calcium salts ($SI = 0$), including amorphous calcium phosphate. The increase in HCO_3^- content (SBFr) leads to dissolution and phase transformation of the amorphous calcium phosphate into more thermodynamically stable salts (Table 3).

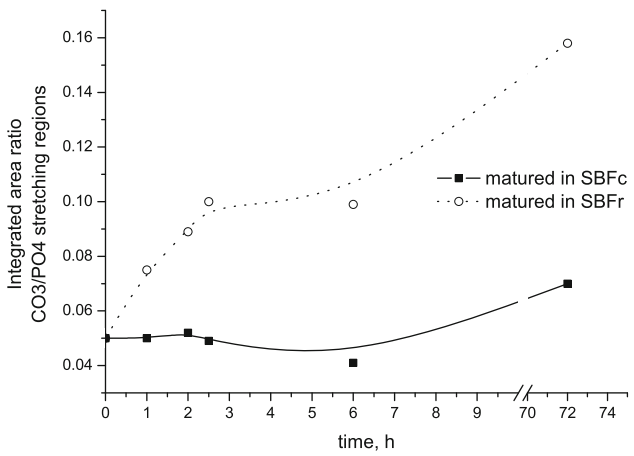

Fig. 6 Changes of the CO_3/P ratio (according to FTIR spectra) in samples matured in SBFc and SBFr

It was calculated that for the equilibrium product (**ACP) there was no influence of HCO_3^- ions, the system tending to thermodynamic equilibrium by dissolution of all the co-precipitated solid phases and re-crystallization of thermodynamically unstable amorphous calcium phosphate (with $SI < 0$) into pure hydroxyapatite (with $SI = 0$) (Table 3).

The model cannot predict the formation of Mg substituted carbonated hydroxyapatite due to absence of data.

The thermodynamic calculations of the solubility of the co-precipitated solid phases ($SI > 0$) (Table 3) with differing contents of HCO_3^- indicate that the increased content of HCO_3^- ions in the solution leads to an increased solubility of the magnesium compounds in contrast to the calcium ones (Fig. 7a). These results determine analogous distribution of magnesium and calcium species (Fig. 7b) in the solution, although the amount of magnesium co-precipitates is too small. The solubility of $Mg(OH)_2$ and $MgCO_3{\cdot}Mg(OH)_2{\cdot}3H_2O$ increase significantly, when slightly for $Mg_3(PO_4)_2{\cdot}8H_2O$. This results in a significant increase in content of the $MgHCO_3^+$ species and in a slight increase of $MgCO_3^0$ and $MgHPO_4^0$ species in the solution (Fig. 7b). Contrary to the magnesium compounds, the solubility of ACP, the dominant phase in the precipitated mixture, and also of $CaHPO_4$ slowly increase with increasing HCO_3^- ions content. However, the high amount of ACP determines the increased amount of $CaHCO_3^+$ species in the solution. The only exception is the solubility of $CaCO_3$ which decreases with the content of HCO_3^- ions, the precipitation starting at HCO_3^- above 6 mmol/l. The solubilities of $Ca_8H_2(PO_4)_6{\cdot}5H_2O$, $Ca_9Mg(HPO_4)(PO_4)_6$ and $Ca_{10}(PO_4)_6(OH)_2$ salts do not depend on the content of HCO_3^- as the used SBFs are supersaturated.

These thermodynamic data explain the results on the maturation kinetics.

4 Conclusion

The kinetic and spectral studies and the thermodynamic simulations of the biomimetic precipitation of XRD amorphous calcium phosphate and its consequent phase transformation into poorly crystalline apatite in two SBFs, differing in their content of HCO_3^- ions, lead to the following conclusions: (i) kinetic reasons determine the

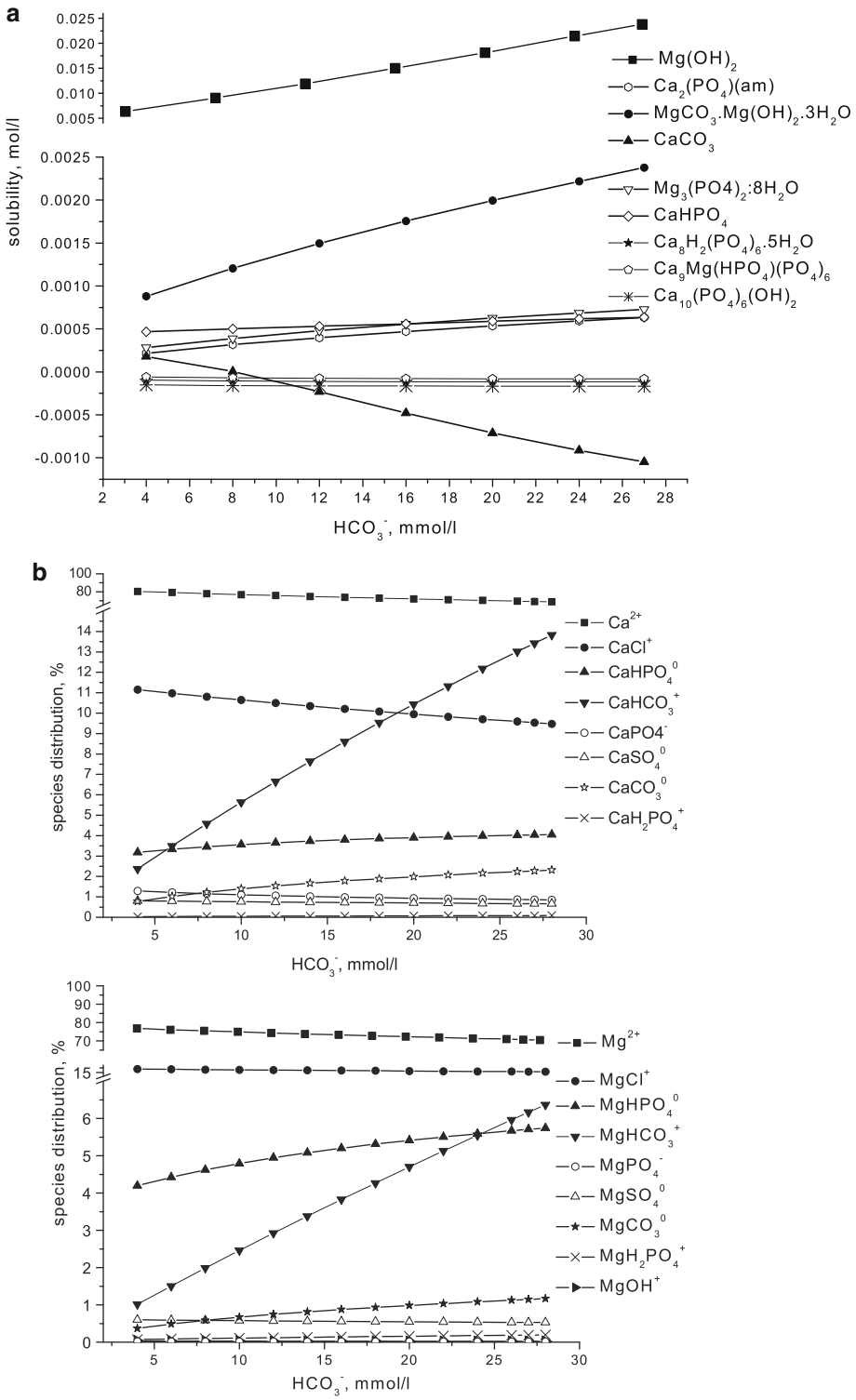

Fig. 7 Thermodynamic calculation of: **a** solubility of all co-precipitated phases (SI > 0); **b** Ca and Mg species distribution in liquid phases

biomimetic precipitation of a XRD amorphous calcium deficient phosphate (ACP) that is less thermodynamically stable in comparison with calcium hydroxyapatite; (ii) precipitated ACP always contains impurities due to the simultaneous co-precipitation of small amounts of magnesium and calcium hydroxides, carbonates etc., ion substitution and maternal liquid incorporation; (iii) the increased content of HCO_3^- ions in the micro-environmental surrounding increases the rate of phase transformation and the concentration of $MeHCO_3^+$ (Me = Ca, Mg) species in the solution, but decreases the solubility of $CaCO_3$ and accelerates its precipitation; (iv) the

biomimetic maturation leads to quick changes in the composition of solid and liquid phases during the first 1–2 h and to simultaneous processes of dissolution/crystallization/re-crystallization that accelerate the phase transformation of less thermodynamically stable amorphous calcium phosphate into poorly crystalline hydroxyapatite.

Having in mind that carbonates are one of the effective buffer systems in the body fluid, the results of this study corroborate the role of carbonate content in SBFs as one of the main factors in the phase transformation of amorphous calcium phosphate.

Acknowledgments This work is financially supported by the Bulgarian Ministry of Education, Youth and Science under Projects DO-02-82/2008 and X-1509.

References

1. Dorozhkin SV. Calcium orthophosphates in nature, biology and medicine. Materials. 2009;2:399–498.
2. Yang Y, Kim KH, Ong JL. A review on calcium phosphate coatings produced using a sputtering process—an alternative to plasma spraying. Biomaterials. 2005;26:327–37.
3. Singh R, Kurella A, Dahotre NB. Laser surface modification of Ti–6Al–4V: wear and corrosion characterization in simulated biofluid. J Biomater Appl. 2006;21:49–73.
4. Jalota S, Bhaduri SB, Tas AC. Effect of carbonate content and buffer type on calcium phosphate formation in SBF solutions. J Mater Sci: Mater Med. 2006;17:697–707.
5. Kontonasaki E, Zorba T, Papadopoulou L, Pavlidou E, Chatzistavrou X, Paraskevopoulos K, Koidis P. Hydroxy carbonate apatite formation on particulate bioglass in vitro as a function of time. Cryst Res Technol. 2002;37:1165–71.
6. Tanahashi M, Yao T, Kokubo T, Minoda M, Miyamoto T, Nakamura T, Yamamuro T. Apatite coating on organic polymers by a biomimetic process. J Am Ceram Soc. 1994;77:2805–8.
7. Girija EK, Yokogawa Y, Nagata F. Bone-like apatite formation on collagen fibrils by biomimetic method. Chem Lett. 2002; 7:702–3.
8. Kokubo T. Surface chemistry of bioactive glass-ceramics. J Non-Cryst Solids. 1990;120:138–51.
9. Bayraktar D, Tas AC. Chemical preparation of carbonated calcium hydroxyapatite powders at 37°C in urea-containing synthetic body fluids. J Eur Ceram Soc. 1999;19:2573–9.
10. Marques PAAP, Cachinho SCP, Magalhaes MCF, Correia RN, Fernandes MHV. Mineralization of bioceramics in simulated plasma with physiological CO_2/HCO_3-bufer and albumin. J Mater Chem. 2004;14:1861–6.
11. Marques PAAP, Magalhaes MCF, Correia RN. Inorganic plasma with physiological CO_2/HCO_3 buffer. Biomaterials. 2003;24: 1541–8.
12. Xiaobo Ch, Yuncang L, Peter DH, Cui'e W. Microstructures and bond strengths of the calcium phosphate coatings formed on titanium from different simulated body fluids. Mater Sci Eng. 2009;C 29:165–71.
13. Hui W, Changjian L, Ren H. Effects of structure and composition of the CaP composite coatings on apatite formation and bioactivity in simulated body fluid. Appl Surf Sci. 2009;255:4074–81.
14. Shibli SM, Jayalekshmi AC. A novel nano hydroxyapatite-incorporated Ni–P coating as an effective inter layer for biological applications. J Mater Sci: Mater Med. 2009;20:711–8.
15. Martin RA, Twyman H, Qiu D, Knowles JC, Newport RJ. A study of the formation of amorphous calcium phosphate and hydroxyapatite on melt quenched Bioglass using surface sensitive shallow angle X-ray diffraction. J Mater Sci: Mater Med. 2009;20:883–8.
16. Krumm, S. An interactive windows program for profile fitting and size/strain analysis. Mater Sci Forum. 1996;228–231:183–188.
17. Parkhurst DL. User's guide to PHREEQC—a computer program for speciation, reaction-path, advective-transport, and inverse geochemical calculations. U.S. Geological Survey Water-Resources Investigations Report 95-4227; 1995. http://wwwbrr.cr.usgs.gov/projects/GWC_coupled/phreeqc/references.htm.
18. Todorov T, Rabadjieva D, Tepavitcharova S. New thermodynamic database for more precise simulation of metal species in natural waters. J Univ Chem Technol Metall. 2006;41:97–102.
19. Fernández E, Gil FJ, Ginebra MP, Driessens FCM, Planell JA, Best SM. Calcium phosphate bone cements for clinical applications. Part I: solution chemistry. J Mater Sci Mater Med. 1999;10:169–76.
20. Sinyaev VA, Shustikova ES, Levchenko LV, Sedunov AA. Synthesis and dehydration of amorphous calcium phosphate. Inorg Mater. 2001;37:619–22.
21. Chow LC, Eanes ED. Octacalcium phosphate. Basel: Karger; 2001.
22. Tas AC. Synthesis of biomimetic Ca-hydroxyapatite powders at 37°C in synthetic body fluids. Biomaterials. 2000;21:1429–38.
23. Betts F, Blumenthal NC, Posner AS, Becker GL, Lehninger AL. Atomic structure of intracellular amorphous calcium phosphate deposits. Proc Natl Acad Sci USA. 1975;72:2088–92.
24. Blumenthal NC, Betts F, Posner AS. Stabilization of amorphous calcium phosphate by Mg and ATP. Calcif Tissue Res. 1977;23:245–50.
25. Chung SY, Kim YM, Kim JG, Kim YJ. Multiphase transformation and Ostwald's rule of stages during crystallization of a metal phosphate. Nat Phys. 2009;5:68–73.
26. Fleet ME. Infrared spectra of carbonate apatites: $\nu 2$-region bands. Biomaterials. 2009;30:1473–81.